Fracture in electrophoretically deposited CdSe nanocrystal films

Shengguo Jia,[1,2] Sarbajit Banerjee,[1,2,a)] Dongyun Lee,[1,3,b)] Joze Bevk,[1,2] Jeffrey W. Kysar,[1,3] and Irving P. Herman[1,2,c)]
[1]*Materials Research Science and Engineering Center, Columbia University, New York, New York 10027, USA*
[2]*Department of Applied Physics and Applied Mathematics, Columbia University, New York, New York 10027, USA*
[3]*Department of Mechanical Engineering, Columbia University, New York, New York 10027, USA*

(Received 15 May 2008; accepted 15 March 2009; published online 21 May 2009)

We have studied the fracture, strain, and stress of electrophoretically deposited (EPD) films of CdSe nanocrystals as a function of the film thickness, nanocrystal size, and drying method. Fracture results from the film stress that develops with the loss of residual solvent after EPD when the film exceeds a threshold thickness that increases with nanocrystal core diameter from ~300 to 1200 nm for core diameters from 2.3 to 5.0 nm, respectively. A hierarchical pattern of wider first generation and then narrower higher-generation cracks is observed after drying and this generational crack formation and a preferred direction for film drying are observed in real time. Delamination is seen to initiate from wider cracks, mostly between the bulk of the film and a very thin layer of nanocrystals strongly bound to the Au-coated silicon substrate. Estimates of the film toughness are made for channel cracking and delamination. © *2009 American Institute of Physics*.
[DOI: 10.1063/1.3118630]

I. INTRODUCTION

Films of colloidal nanocrystals hold a promise for several applications. For example, CdSe/ZnS core-shell nanocrystals have been assembled layer by layer on InGaN/GaN light-emitting diodes to produce white light sources.[1] Photodetectors with a sandwich geometry and active in the visible spectrum have been developed using CdSe nanocrystal films.[2] Thin films of CdSe and CdTe nanocrystals have been utilized to produce ultrathin donor-acceptor solar cells.[3] However, the formation of such high quality films remains a challenge. Indeed, the use of these films often hinges on whether their mechanical properties, chemical stability, and electrical properties are acceptable for the specific application, and, if they are not, on how they can be improved. The purpose of this work is to address the mechanical integrity of nanocrystal films fabricated by electrophoretic deposition (EPD) and to establish the source and extent of the failure mechanisms that lead to fracture in these films when they are very thick. This should lead to a better understanding of the mechanical integrity of all films composed of nanocrystals and should stimulate the development of new experimental approaches to improve mechanical integrity.

One reason for the observed experimental difficulties with nanocrystal films is the complex nature of these films, which are composed of nanocrystal cores capped with ligands and the common unavoidable presence of voids, which may contain residual solvent after film formation. There are several types of interfaces in such films, each with nanometer characteristic lateral dimensions, such as those between the cores and ligands, between the ligands on neighboring nanocrystals, and those between ligands and potential voids. This complex overall structure and interface structure can strongly impact film properties, and in particular, the film mechanical properties, so the bonding between the ligands and other species is critically important. In particular, the tendency to crack, observed in many nanocrystal films and the subject of this study, has to be better understood and controlled through studies of the formation and propagation of the cracks in the films that have ultimately failed.

In Ref. 3, we showed that films of CdSe nanocrystals with ~3 nm core diameter, capped by trioctylphosphine oxide (TOPO)/trioctylphosphine selenide (TOPSe) that are formed by EPD in solution, fracture after removal from the solution when they are grown above a certain critical thickness. Presumably, this arises from residual stresses that appear after the evaporation of the residual solvent. We showed in Ref. 4 that the in-plane strain and stress in such films can be quite large before they fracture by using Raman microprobe spectroscopy to measure the strain in the CdSe cores and analyzing the fracture patterns to estimate the average film strain. We then used nanoindentation in Ref. 5 to show that these films are viscoplastic and to determine the film elastic modulus of the dry film (~10 GPa). The elastic modulus determined using nanoindentation (in which the film was compressed) was consistent with that deduced in the previous study (in which the films were under tension[4]). Moreover, in the nanoindentation studies the modulus was found to be the same within experimental error near and far from the cracks, corresponding to relatively more and less stress-relieved regions.

To better understand the cracking behavior in these films, we have studied the fracture patterns of EPD films as a

[a)]Present address: Department of Chemistry, University at Buffalo, Buffalo, NY.
[b)]Present address: Materials Science and Engineering Division, Korea Institute of Science and Technology, Seoul, Korea.
[c)]Author to whom correspondence should be addressed. Electronic mail: iph1@columbia.edu. Tel.: 1-212-854-4950. FAX: 1-212-854-1909.

function of film thickness, nanocrystal size, and drying method, and have analyzed these findings using existing theories of the fracture of homogeneous films due to residual stress.

II. EXPERIMENTAL METHODS

CdSe nanocrystals were synthesized as detailed previously, following the recipe of Murray *et al.*[6] Nanocrystals with 2.3, 3.2, and 5.0 nm core diameters capped by TOPO/TOPSe were used with the core diameters determined from the wavelength of the first exciton peak in absorption.[7] To optimize film quality, these three sizes of nanocrystals were washed (reprecipitated) for 4, 2, and 2 cycles, respectively, before EPD.[8,9] (Washing cycles are expected to somewhat decrease the number of surface ligands, as is described in Refs. 8 and 9.) Deviation from the cited optimum number of precipitation cycles was found to increase the film surface roughness.[9] If extra ligands were added back to the solution before deposition using particles washed the optimum number of times, the film would often have very poor quality or not form at all, depending on the amount of TOPO added.[3,8,9]

Unless otherwise specified, EPD was performed on electrodes composed of 150 nm thick Au films deposited by thermal evaporation on a Cr adhesion layer atop an $\sim 2 \times 1$ cm^2 region on (100) silicon. In optical microscopy transmission experiments, indium tin oxide (ITO)-coated glass (Delta technologies, surface resistance is $\sim 5-10\ \Omega$) electrodes were used. Two electrodes were placed facing each other and separated by ~ 2 mm to simulate a parallel-platelike geometry. In a typical experiment, twice-washed 3.2 nm CdSe nanocrystals were dissolved in a nonpolar solvent (hexane/octane, v/v, 90%/10%) with a nanocrystal concentration of $\sim 10^{14}$ dots/cm^3. Almost identical uniform CdSe nanocrystal films were deposited on both electrodes upon the application of a 500 V dc voltage. For very thick films, variations in run-to-run thickness were due to slight variations in the particle charge distribution, as described in Ref. 8. (Among the many runs performed, there was great consistency in the observation of the critical thickness for which fracture is first seen, which was not related to any run-to-run variations in film thickness.) A similar protocol was also used to fabricate nanocrystal films using 2.3 and 5.0 nm diameter nanocrystals.

Optical microscopy images were recorded using a Nikon Eclipse microscope to determine the crack widths and spacing between the cracks for EPD films deposited on Au electrodes, and in some cases video microscopy images were recorded to view the crack formation for films deposited on ITO film on glass (Mitutoyo microscope). To facilitate video imaging, the crack propagation speed was decreased by using nanocrystal solutions with isopar G (a mixture of branched aliphatic hydrocarbons with a vapor pressure lower than that of hexane from Exxon), decane, or undecane during EPD. The crack microstructure was investigated by scanning electron microscopy (SEM) and energy dispersive x-ray (EDX) spectroscopy on a Hitachi 4700 instrument.

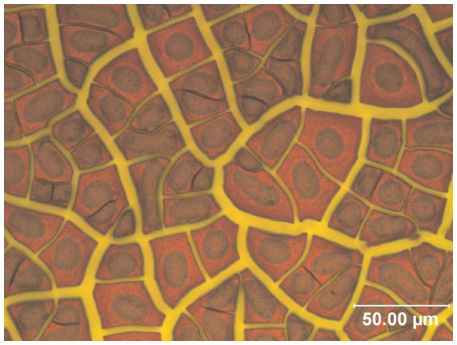

FIG. 1. (Color online) Micrograph of 2500 nm thick 3.2 nm CdSe nanocrystal EPD film. The scale bar is 50 μm wide.

III. RESULTS

Films above and below the threshold thickness for channel cracking were deposited. Nanoindentation[5] was used to determine the elastic moduli of the 2.3, 3.2, and 5.0 nm CdSe nanocrystal films to be 5.0, 10.0, and 14.0 GPa, respectively.

A. Fracture patterns and threshold thickness

For films above the threshold thickness, the local fracture geometry was generally the same for 3.2 nm diameter nanocrystal films of the same thickness allowed to dry by four different methods; however the overall pattern over the entire ($\sim 1 \times 1.5$ cm^2) film varied with method (see supplemental material, Fig. S1, Ref. 10). Under no drying condition was the degree of fracture significantly lessened. For fast dried and slow dried films the major channel cracks were preferentially along the vertical direction of the drying front. Visual observation showed that the cracks propagate from the top of the drying film to the bottom. This was also seen under a microscope when the electrodes were lifted part way from the solution and then the film dried slowly. For drying on a flat surface (horizontal drying and annealing in hexane solvent), the major channel cracks point radially to the center of the film. Video microscopy (below) of "horizontal drying" with isopar solvent showed preferential drying from the physically higher to lower regions for these substrates that were slightly tilted from the horizontal.

Most studies were conducted on fast dried films with the presented micrographs and SEMs from typical regions near the center of the film after drying for 30 min to 8 h. Films grown on the positive and negative electrodes have the same thickness and dry with the same fracture patterns.

The fast dried films fracture when they are thicker than a threshold thickness. Several generations of cracks are typically seen in many fractured films. Figure 1 shows an optical image of a 2500 nm thick 3.2 nm CdSe nanocrystal film, which is much thicker than the threshold thickness of ~ 900 nm. There are at least three "generations" of cracks in these films as characterized by crack widths. The widest cracks, called "first generation" cracks, are usually $\sim 4-8$ μm wide and spaced at $\sim 30-50$ μm apart in this case, which is ~ 20 times the 2500 nm film thickness. The "second generation" cracks are $\sim 2-4$ μm wide and spaced at $\sim 15-30$ μm apart, which is ~ 10 times the film thickness. Some much narrower "third generation" cracks that are

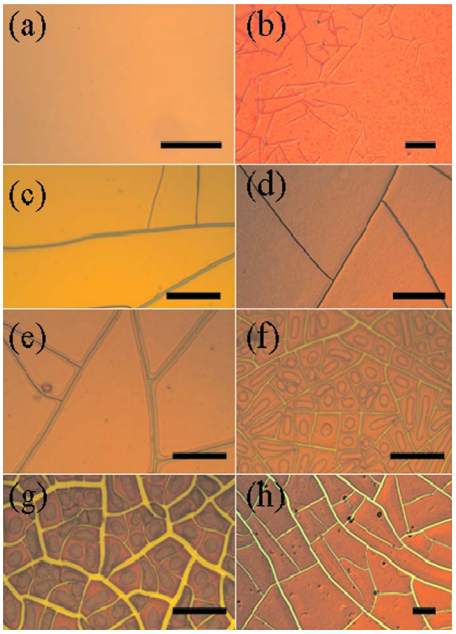

FIG. 2. (Color online) Micrographs showing crack patterns in different 3.2 nm CdSe nanocrystal EPD films with film thicknesses of (a) 600, (b) 900, (c) 1000, (d) 1600, (e) 2000, (f) 2300, (g) 2500, and (h) 3200 nm. The scale bars are all 50 μm wide. The crack, delamination, and undelaminated area fractions for all studied fractured 3.2 nm nanocrystal films average to 20%, 39%, and 41%, respectively.

only about ~1 μm wide or narrower can also be found (and are seen by SEM) and are spaced at ~5–10 μm apart. The typical island dimensions range from ~10×15 to 20 ×30 μm^2 for the 2500 nm thick film.

The thicker the film is above threshold, the more extensive is the cracking with more cracks, the wider the cracks, and the more the generations of cracks (Fig. 2). Just above threshold [900 nm, Fig. 2(b)] there is sometimes an extensive mesh of cracks that may not fracture down to the Au substrate. These cracks get deeper for thicker films [as in Fig. 2(g) for 2500 nm films]. Much thicker films show wider and longer first generation cracks and more pronounced higher generation crack structure. In thinner films [900–1600 nm thick, Figs. 2(b)–2(d)] there is only one generation of cracks, while in thicker films there are at least two generations of cracks. Higher generation cracks do not exhibit the direction preference of first generation cracks but tend to intersect first generation cracks at right angles.

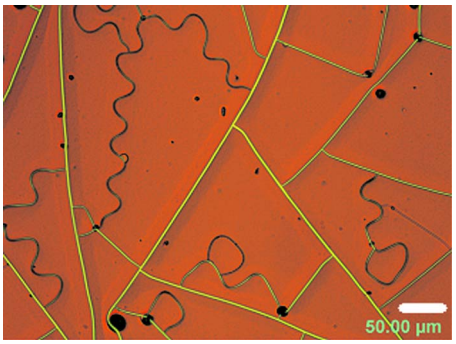

FIG. 3. (Color online) Micrograph showing channel and oscillatory cracks coexist in one 3500 nm thick 3.2 nm CdSe nanocrystal EPD film. The scale bar is 50 μm wide.

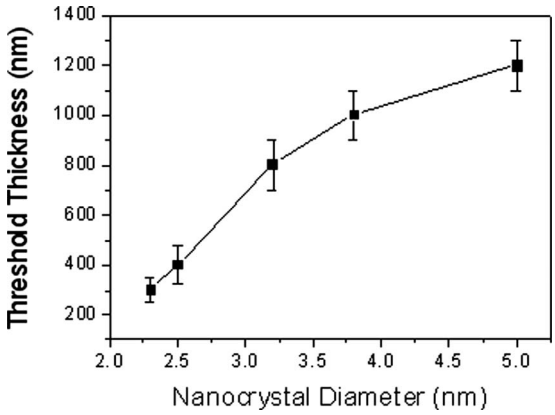

FIG. 4. Threshold thickness of EPD films vs nanocrystal core diameter.

In a few cases, second generation oscillatory cracks were seen in addition to the first generation linear channel cracks (Fig. 3). It was not possible to find a set of conditions that consistently produced these oscillatory cracks. The first generation channel cracks are ~4.0–7.0 μm wide and spaced by 80–200 μm. The second generation oscillatory cracks are ~1.5–3.0 μm wide and spaced by ~50–100 μm.

The threshold thickness for cracking of the nanocrystal films increases with the size of the nanocrystals (Fig. 4). Examples of very thick films, which are much thicker than the critical thickness, are shown in Fig. 5 for three particle sizes. (The thickest film possible by EPD was grown in each case[8] to examine the maximum strain relief in the films.) The different colors of the film arise from the varying absorption edge as a function of the nanocrystal size.

After baking at 80 °C under nitrogen for 30 min, a 600 nm thick EPD film of 3.2 nm CdSe nanocrystals shrinks to 400 nm.

B. Crack microstructure

The SEM images of first generation channel cracks in very thick fast dried films show that the film is delaminated (or debonded) from the substrate in the vicinity of the cracks (Fig. 6). The angle of delamination is ≤1.5°, and this has been confirmed by atomic force microscopy (AFM),[4] and the extent of delamination depends on the local geometry and width of the cracks. Optical microscopy also shows that the edges of the film near the crack are slightly higher than the adhering parts of the film. Still, this angle is small enough

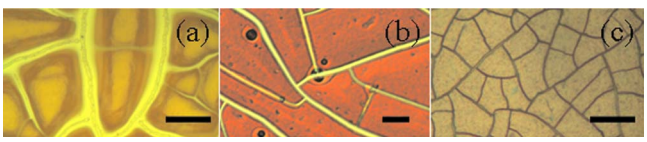

FIG. 5. (Color online) Micrographs showing crack patterns in very thick nanocrystal EPD films with different CdSe core sizes: (a) 1600 nm thick 2.3 nm nanocrystal film, (b) 3200 nm thick 3.2 nm nanocrystal film, and (c) 2500 nm thick 5.0 nm nanocrystal film. The scale bars are all 25 μm wide. The crack, delamination, and undelaminated area fractions for the 1600 nm thick 2.3 nm nanocrystal films, as in part (a), average to 37%, 38%, and 25%. In part (c), the crack and film area fractions for the 2500 nm thick 5.0 nm nanocrystal film are 17% and 83%. (See Fig. 2 caption for more on part (b)).

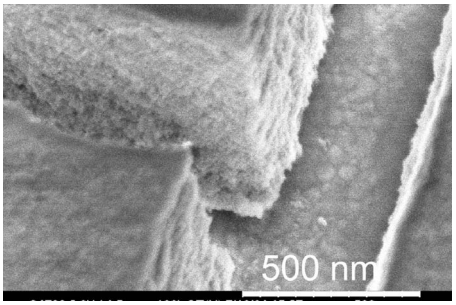

FIG. 6. SEM picture of a crack in the 3200 nm thick 3.2 nm CdSe nanocrystal EPD film shows the layered structure of the film. The scale bar is 500 nm wide.

that the observed crack width is very nearly equal to the width of the crack if there were no bending. For very thick (>2500 nm) films, the films can be delaminated for up to 25 μm from the channel cracks. In Fig. 1, the delaminated regions are red and the regions in contact with the substrate appear to be brown (and the exposed substrate is yellow).

SEM and EDX imaging indicate that a thin layer of 3.2 nm CdSe nanocrystals adheres to the substrate within much of the region of the larger cracks (~15–20 μm wide) in very thick films (3200 nm) (Fig. 7).[4] These very thin CdSe nanocrystal layers have been determined by Raman microprobe analysis[4] to be under high tensile strain (which is reasonable given the strong adhesion of these layers to the substrate). EDX and Raman measurements indicate that there are narrow cracks (~1–3 μm) within these thin CdSe nanocrystal layers, and the bare Au film substrate appears as a stripe in the crack, as is also seen in the SEM in Fig. 7(b) and also in some optical micrographs [as in Fig. 5(a) for 2.3 nm nanocrystal films]. Cross-sectional SEM images of the cracks provide further evidence that these films have a layered structure (Fig. 6).

C. Crack propagation

Optical microscopy of very thick films deposited on ITO films on glass electrode assemblies, which were only partially but rapidly pulled out of the hexane/octane solvent and then allowed to dry slowly, indicates that crack formation begins within ~20 s upon removal. The regions of the film farthest from the solvent meniscus are seen to be the most heavily cracked, and all the cracks are seen to terminate less than 1 mm above the meniscus [where the solvent vapor pressure is high; the vapor pressures of hexane and octane are 190 and 19.3 mm Hg at 300 K (Ref. 11)]. This demonstrates that films do not fracture in solution but only upon removal from the solvent.

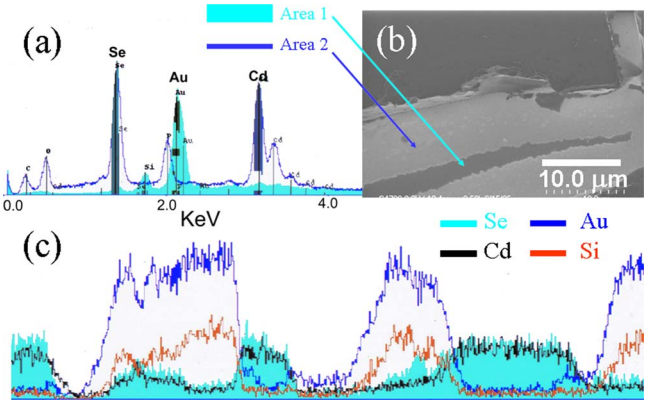

FIG. 7. (Color online) Within a wide crack in the 3200 nm thick 3.2 nm CdSe nanocrystal EPD film: (a) EDX spot analysis of the central stripe region (area 1) and surrounding stripes on either side (area 2), (b) SEM picture with a 10 μm wide scale bar of this central darker gray stripe surrounded by lighter gray stripes, and (c) EDX line scan across this wide crack. This shows that the central strip is the Au film and the adjacent strips are very thin layers of CdSe nanocrystal films on the Au film.

An optical microscope video of drying was obtained for 3.2 nm CdSe nanocrystal EPD films deposited on Au with a solvent isopar G, which evaporates slower than the hexane/octane mixtures used for other studies presented, but which generally leads to the same crack pattern after drying. Using this solvent, the 2800 nm film begins to crack after 2 min, the drying front moves at a speed of ~10–20 μm/s (on the basis of the formation of advancing channel cracks), and crack formation ceases at ~5–10 min after the beginning of drying. For the most part, the widest cracks are those that are among the first to nucleate and form at the drying front. They form as narrow cracks and the crack front propagates as a narrow crack moving in one direction along the dominant drying direction (in the general direction of the drying front) at speeds of ~20–30 μm/s. At the same time, the previously formed crack widens (in ~2–4 s). It is not clear if the delamination that is seen later occurs at the same time as the crack formation or if there is first the film detachment that must occur with crack widening and then the slight curlup [≤1.5° (Ref. 4)] occurs, which is seen in the delamination.

Other cracks form in between these wide cracks and propagate as narrow cracks in opposite directions (~20–30 μm/s) until they reach existing wider cracks; before they reach these wider cracks the secondary crack fronts slow down and gradually change direction until they are normal to the existing cracks. In some cases the cracks approach but do not reach a major crack. (Such dangling cracks are more commonly seen in slow drying.)

IV. DISCUSSION

A. General observations on drying and fracture

Fracture occurs only during drying and not while the films are in solution. With the film still in solution after EPD, there is no (or very little) stress in the film and the film adheres to the substrate. Solvent is trapped in the interstitial regions between the nanocrystals and likely interpenetrates the ligand shell; for larger ligands and smaller cores, some of the ligands can also extend to occupy these interstitial regions. As a result of drying of this poroelastic material, some or most of the solvent is gone from the interstitial regions and within the ligand regions, leaving behind nanovoids. Since the equilibrium distance between cores is smaller after the loss of residual solvent, this results in an intrinsic strain and stress in the film. The residual stress may be even larger for loosely packed films and films with larger ligand-to-core volume ratios (i.e., smaller cores) because they initially contain relatively more solvent. For hard-sphere core/ligand nanocrystals, the packing fractions f are 0.64 and 0.58 for

random close-packed and random loose-packed structures, respectively.[12,13] Ligand interdigitation would decrease this solvent (void) fraction from this ~0.4 (i.e., 1 – ~0.6 hard sphere estimate), while swelling due to ligand/solvent interactions would tend to increase it.

The physical properties including the stress, strain, modulus, and toughness of the drying films exhibit both a spatial and time dependence that reflect changing solvent concentration during the drying process. The first cracks appear when the elastic strain energy per unit volume of the material exceeds the toughness of the material, so new surfaces can be created. In the drying of films thicker than the critical thickness, film fracture occurs first from the "top" of the film surface and then proceeds down to the "bottom" of the film to form channel cracks because evaporation of solvent starts at the top and so stress develops there first and then lower in the film. Once the cracks are formed, the solvent loss through the crack walls and particularly the crack tips greatly influence—if not dominate—the fracture dynamics.

Once the cracks reach the interface, at some point the partially delaminated film at the bottom of the channel cracks will exceed the critical crack length, after which the islands between channel cracks will be prone to delamination. This debonding appears to occur from a very thin layer of nanocrystals which continues to adhere to the Au film, which suggests the adhesion between the Au surface and the nanocrystals is stronger than that between layers of nanocrystals. It is likely that the Au stripes sometimes seen in the crack regions result from fracture of this adhering layer and not from the initial debonding from the Au layer, followed by continued debonding from an adhering layer of nanocrystals. The fracture between nanocrystals in the channel and in delamination cracks is likely between the ligands of neighboring nanocrystals, but fracture between the ligands and core cannot be discounted.

For films much thicker than the threshold thickness, fracture continues with higher and higher generation cracks forming until the cracks approach each other sufficiently close that there is not enough strain energy in the remaining volume to drive the fracture further. Higher generation cracks nucleate in between lower generation cracks because the stresses are largest there (and larger than near the cracks). The crack propagation speed decreases when it approaches other cracks because the stress is more relieved there and its direction becomes normal to the other cracks so that the crack maintains no shear stress relative to the prolongation of the crack tip. When higher generation cracks approach but do not reach a major crack (dangling cracks), as is more commonly seen in slow drying, stress has been relieved enough that there is not enough residual stress for continued crack propagation. The second-generation oscillatory cracks only occasionally seen in these films under tension have been seen in other films under tension at times[14] and are more commonly seen in compression where they correspond to buckling and are called telephone cords.[15] They are thought to arise from differential drying rates.

In Figs. 1 and 2(g), the several generations of channel cracks appear as yellow stripes due to light reflection from the largely exposed Au substrate. Within the islands defined by these cracks are brown regions that are often surrounded by red regions. These red regions are likely delaminated films surrounding brown quasiellipsoidal regions where the film may be adhering and the film has the same strain as it had before fracture and with the ellipsoids usually aligned along the longest dimension of irregularly shaped regions. Delamination is also suggested in Fig. 5(a) for 2.3 nm nanocrystal films and Fig. 2(f) for 3.2 nm nanocrystal films. Delamination likely occurs in Fig. 2(h) for 3.2 nm nanocrystal films and possibly in Fig. 5(c) for 5.0 nm nanocrystal films, for which there is no localized structure because the films are optically thick. Little film delamination is suggested in Fig. 2(e).

B. Modeling mechanical behavior

Film toughness is related to residual film stress before fracture using the equilibrium crack spacing in films, the threshold film thickness for fracture, and propagating crack termination (perhaps near an edge or another crack). In each case the toughness is estimated assuming that the critical fracture condition, such as attaining a threshold condition, is met by the film after drying; this is admittedly uncertain because these conditions may actually occur during drying.

1. Fracture theory

Classical fracture theory usually assumes that residual stress builds up rapidly and uniformly in the homogenous film. When films are grown or deposited at elevated temperatures, stress builds up uniformly during cooling in the film due to thermal mismatch. However, fracture can occur even during cooling, so stress buildup can continue away from cracks that have already formed. When EPD films dry, the stress increases with time and builds up faster near the surface than near the substrate, and so it is not uniform in the film. Even so, useful insight is obtainable by using classical fracture theory.

The channel cracks are mode I cracks. The delamination has a mixed mode I and mode II crack character and is characterized by the mode mixity parameter or phase angle ψ that is zero for purely mode I character.

The criterion for crack advance is $G > \Gamma$, where G is the energy release rate and Γ is the *toughness* of the material (sometimes called the fracture resistance or energy). For mixed mode conditions, $\Gamma = \Gamma(\psi)$, which is a minimum under pure mode I conditions ($\psi = 0$) for the channel cracks and larger for the delamination. (For cases where fracture occurs between nanocrystals for both modes with the same plastic contributions, see later.)

The condition for fracture threshold is $G_{th} = \Gamma$. The crack can propagate in steady state with the steady-state release rate $G_{ss} > \Gamma$ and then terminate when the steady-state release rate G_{ss} decreases to $G_{term} = \Gamma$, such as when the crack advances to where the elastic strain energy has been exhausted (e.g., near an edge or another crack, resulting in dangling cracks).

The energy release rate can be expressed as

$$G = \frac{Z\sigma^2 h}{E'}, \tag{1}$$

where Z is a dimensionless parameter,[15] h is the film thickness, and E' for channel cracks is the film plane strain modulus [$=E/(1-\nu^2)$, where E is the elastic modulus and ν is Poisson's ratio], which assumes a linear-elastic constitutive behavior. Such conditions for fracture threshold can be presented in terms of the threshold film thickness h_c for the growth of a single crack in a film from the $G_{\text{th}}=\Gamma_{\text{channel}}$ condition[16]

$$h_c = \frac{\Gamma E'}{Z\sigma^2}. \tag{2}$$

2. Film strain and stress

The equibiaxial in-plane stress in unfractured nanocrystal films is $\sigma=\varepsilon E_{\text{biaxial}}=\varepsilon E/(1-\nu)$, where E_{biaxial} is the biaxial modulus, E is the elastic modulus, and ν is the Poisson ratio of the nanocrystal film. (This assumes a linear dependence of stress on strain, which is expected to be valid only for small values of strain.) In previous work,[4] the average residual film stress was deduced to be 1.6 GPa for the dried 3.2 nm nanocrystal EPD films from the Raman analysis of the strain in the CdSe cores. This value is used here along with the measured elastic modulus and an estimate of the Poisson ratio of $\nu=0.3$. It is assumed that stress is independent of thickness (aside from the stress relief from fracture).

Strains in the unfractured films are estimated by the strain relaxation in films that fracture. Say channel cracks to the substrate develop at the edges of a square region of film of width L_0 and after symmetric partial delamination the film in this island contracts to a square of width L, and symmetrically within this region a square portion of the film of width D still adheres to the substrate. Inside the inner square of width D the film retains the residual strain and outside this square the film has no strain (normal to the edges) within the square of width L. The stretch ratio of a section of film before delamination (strained) relative to that after delamination (unstrained) λ is $(L_0-D)/(L-D)$ in the x and y directions. The biaxial Lagrangian strain in the fully strained film is then $\varepsilon=(\lambda^2-1)/2$.[17,18] In a checkerboard tiling of such square islands, the crack widths are L_0-L. The fractions of areas occupied by cracks, delaminated film regions, and adhering film regions are $(L_0^2-L^2)/L_0^2$, $(L^2-D^2)/L_0^2$, and D^2/L_0^2, respectively. The Lagrangian strain is calculated for several thick cracked films (with visible central adhering regions) using the measured average fractional areas for these three types of regions (which are actually irregularly shaped and sized) in the relations for idealized square tiling.

The Lagrangian strain before fracture from several fractured 3.2 nm nanocrystal films averages to ~0.39 with an uncertainty of $\sim\pm0.2$. (The strains from different films were averaged here; using the averaged fractional areas given in the caption to Fig. 2 to determine strain gives 0.50.) Using $E=10.0$ GPa in a linear constitutive equation leads to an unrealistically large value of stress (5.6 GPa), much larger than that obtained in Ref. 4 of 1.6 GPa (and which is used here).

The channel cracks grow into existence while the material is at least partially saturated. The delamination cracks then are nucleated from the tips of the channel cracks near the substrate, and the delamination also proceeds while the film is at least partially saturated. Since the film is a porous material, part of the characterized strain is introduced first due to a release of the stresses in the film after which the remainder of the strain occurs simply due to the drying process. On the other hand, in order to characterize the toughness of the dry films, it must be assumed that the saturated film is first dried (while the lateral dimensions remain constant because it is constrained to the substrate) after which strain occurs due to the release of stress upon fracture. If our system were a linear poroelastic material,[19,20] the final strain in the system would be independent of the order of the stress release and the drying processes. However, in our system, we assume that the stiffness of the saturated matrix (i.e., CdSe and TOPO) is less than the stiffness of the matrix in the dried state due to interactions of the solvent with the TOPO, so we cannot assume a linear poroelastic behavior. Consequently, it is very likely that the strain we characterize as about 0.4 is a severe overestimate of the strain that would occur upon delamination of a dried film. Therefore, we do not use this value in our calculations of the film toughness. Rather, we rely on independent measurements we have previously made of both the stress in the dried films as well as the elastic properties of the dried films.

The 2.3 nm nanocrystal films have a measured strain of ~0.98 (uncertainty of $\sim\pm0.15$), which is clearly larger than the strain in 3.2 nm nanocrystal films. This is reasonable because the ratio of ligand-to-core volume is larger for smaller cores and ligand swelling by the solvent during EPD would be larger, and the resulting strain would be larger after solvent evaporation. Since the undelaminated area fraction cannot be determined from the 5.0 nm nanocrystal film in Fig. 5(c), only a lower limit to the strain can be determined as 0.10.

3. Film toughness and stress

Three different theories are used to relate the film fracture toughness to the residual film stress, assuming that the specific conditions for fracture are met only after drying.

a. Channel crack equilibrium distribution The theory in Ref. 21 interrelates film thickness, equilibrium average crack spacing, toughness, prefracture stress, elastic modulus, and Poisson's ratio by minimizing the free energy. It applies to channel cracks that do not reach the surface, so it is applicable to film thicknesses just above the critical thickness and is applied here only to the 900 nm thick EPD film of 3.2 nm cores (Fig. 2(b)) for which the average crack spacing is 36.5 μm. Using the ratio of crack separation to film thickness of 40.6 and the Dundurs parameters (α and β) (Ref. 21) and other parameters (see supplemental material),[10] then $\Lambda=0.057$, $\kappa_1=1.8$, $\kappa_2=2.1$, $\alpha=-0.88$, and $\beta=-0.25$. Fig. 5 in Ref. 21 gives a value of $Z=1.16$ (based on $\alpha=-0.75$ and $\beta=\alpha/4$) that can be used along with Eq. (1) to estimate the energy release rate of the film upon channel cracking assuming a threshold thickness of 800 nm and the biaxial stress of 1.6 GPa. Accordingly, the fracture toughness is estimated to

be $\Gamma_{channel}=220\ J/m^2$. (Use of equilibrium theory is reasonable because just above the critical thickness, crack nucleation and propagation are relatively slow.)

b. Channel crack threshold and critical film thickness In Eq. (2), $Z=1.17$ for the threshold formation of channel cracks,[15] according to Ref. 22 (based on $\alpha=-0.90$ and $\beta=\alpha/4$). Using the film stress of 1.6 GPa, threshold film thickness of 800 nm, and other given parameters, $\Gamma_{channel}$ is again $220\ J/m^2$ for films composed of 3.2 nm core sizes.

c. Termination of delamination fracture propagation The initial formation of channel cracks influences the drying process near the substrate (and the concomitant formation of large strains and stress there) so much that these cracks extend to the substrate very fast and lead to delamination so fast that other channel cracks are not formed locally, which likely means that delamination cracks occur while the film is still partially saturated. They are formed elsewhere later when drying is complete elsewhere. Ref. 15 gives $Z=1.028$ for delamination initiation and 0.5 for delamination steady state propagation in Eqs. (1) and (2), but for the analysis of delamination termination we turn to Ref. 23.

In the square tiling approximation of fracture islands in EPD films, channel cracks develop a distance L apart on opposite sides of the square, delamination proceeds, and then it terminates when they are separated by a distance D. Ref. 23 analyzed the convergent debonding of linear strips of films on substrates and related the final separation of the delaminated regions to the initial residual stress, film thickness, and delamination fracture toughness. This one dimensional separation is analogous to the width D of the remaining bonded region in the converging two-dimensional delamination of the EPD films. Within the fracture islands in these 2500 nm thick films of 3.2 nm nanocrystals there are often quasiellipsoidal bonded islands with an average area of $150\ \mu m^2$ (Fig. 1), and so in this quasi-one-dimensional analog of these squares $D=12\ \mu m$. For this $D/h=4.8$ and the Dundurs parameter $\alpha=-0.88$, Fig. 4a in Ref. 23 shows that $G/G_{ss}=0.84$, so $Z=0.84/2=0.42$, and so the delamination toughness is $\Gamma_{delam}=0.42(1-\nu^2)\sigma^2h/E$. (The results are very insensitive to the value of the β Dundurs parameter.) Assuming a Poisson's ratio of 0.3 and a film stress of 1.6 GPa, then Γ_{delam} is $245\ J/m^2$. The results are similar if the islands are modeled as circles of area $150\ \mu m^2$. With $D=14\ \mu m$, then $G/G_{ss}=0.87$, and this results in $\Gamma_{delam}=250\ J/m^2$. Figure 4b of Ref. 23 suggests a mode mixity of about $\psi\approx 40°$.

d. Assessment of film toughness The crack spacing and film threshold methods give $\sim 220\ J/m^2$ for $\Gamma_{channel}$ in 3.2 nm nanocrystal EPD films, and the delamination termination method gives $\sim 250\ J/m^2$ for Γ_{delam} in these films. Given the limited accuracy of the methods, these three results are consistent with each other. (As discussed below, the toughness for channel cracks and delamination could be expected to be quite different.) These values represent the toughness of an unstrained film. (The strained films resulting from EPD are more brittle.) Other than the large experimental uncertainties in determining the stress and strain in the films, there are two major uncertainties in this approach. (1) This analysis is flawed if the threshold for channel cracking and/or delamination termination is more easily met by the drying film than by the dried film. This is unknown. (2) Even in analyzing the dried films, Eqs. (1) and (2) assume a linear relation of stress and strain, and this is not likely valid for this composite material. While independent measurement of toughness and the constitutive relations await future experiments on free-standing films, the impact of the second point can be considered a bit further.

The more general form of Eq. (2) is $h_c=\Gamma/2ZW$, where W is the elastic strain energy density released due to fracture. While there is no existing closed form solution for channel cracking in nonlinear elastic materials, we can estimate the difference in the stored elastic strain energy densities for different constitutive models. If $Z=0.5$, Eq. (1) represents the energy release rate due to the delamination of a thin film from a substrate; during this process, the film changes from a state of equibiaxial tension of magnitude σ to a state of uniaxial tension of magnitude $(1-\nu)\sigma$ so that the value of strain in the uniaxial direction is the same as for the biaxial state. Based on a thickness of 800 nm, the energy release rate due to delamination is $93\ J/m^2$ for the assumed stress, elastic modulus, and linear constitutive model. Another possible constitutive relationship that can be used to model this film is the Arruda–Boyce model,[24,25] which is valid for neo-Hookean rubberlike materials. Using values of locking stretch ratio of 1.1 and stress prefactor of 620 MPa in the Arruda–Boyce model gives a tangent modulus of about 10 GPa under uniaxial tension at a true strain of about 0.1, along with a biaxial stress state of about 1.6 GPa, so that these parameters give a reasonable description of the experimental results. For such a material, the energy release rate due to delamination in going from a state of equibiaxial tension to a state of uniaxial tension (with the same stretch ratio) is $48\ J/m^2$, assuming a thickness of 800 nm. Therefore, the calculated energy release rate from the linear model is essentially twice that of the Arruda–Boyce model, which may give an indication of the overestimate of the channel cracking and delamination toughness estimates presented here. Also, using the elastic modulus in Eq. (2) as determined by nanoindentation (which is measured after the film has been compressed) may also introduce errors in determining the toughness.

This toughness is $\Gamma=2\gamma_s+\gamma_p$ for fracture within one material, where γ_s is the surface free energy and γ_p is the energy dissipated by plastic deformation per unit area of crack advance. Fracture likely affects the bonds between ligands of neighboring particles and possibly the core-ligand bonds but not the cores themselves. The surface energy associated with the crack formation in EPD films due to breaking the ligand-ligand bonds is estimated to be $2\gamma_s=mBFLn^{2/3}$. The areal density of nanocrystals is $n^{2/3}$, where n in the density of nanocrystals (with $n=3f/4\pi r^3$ and r is estimated as the core radius plus the thickness of the ligand shell, ~ 1 nm), and the packing fraction is $f\sim 0.6$. The numbers of ligands per core L are 55, 205, and 481 for the 2.3, 3.2, and 5.0 nm nanocrystal films.[8] The fraction of ligands on the core that fractures is F, which is taken at its upper limit of 0.5. There are m interactions between two ligands, each with average bond strength B. Assuming the TOPO ligand-ligand bonds that break in the fracture of EPD films interact dominantly

by van der Waals interactions, B is ~5 kJ/mol (Ref. 26) and $m=24$ (one for each carbon atom in TOPO or TOP), and the estimates for $2\gamma_s$ are 0.32, 0.83, and 1.07 J/m^2 for the 2.3, 3.2, and 5.0 nm nanocrystal EPD films, respectively. These are two orders of magnitude smaller than the values of $\Gamma_{channel}$ determined here. Higher estimates of the toughness, respectively 2.9, 7.4, and 9.6 J/m^2, are obtained assuming even stronger C–C covalent bonds with strength B ~357 kJ/mol (Ref. 27) with $m=3$ (three alkyl chains per ligand), which are still an order of magnitude smaller than the determined values of $\Gamma_{channel}$.

Such a large difference between $\Gamma_{channel}$ and $2\gamma_s$ as this would indicate that $\gamma_p \gg 2\gamma_s$, and that dissipative processes during fracture dominate,[16] which could include thermal energy, the relaxation of the position of nanocrystals near the surface, or the reconstruction of the nanocrystals to match up available bonds near the surface. Moreover, some or most of this difference could be due to an overestimate of $\Gamma_{channel}$ as discussed earlier. However, irrespective of the details of the microscopic model discussed here, we believe the high values of fracture toughness of these films reflect their high yield stress as determined experimentally by nanoindentation.[5]

Because the fracture mode mixing is large in delamination, the mode mixity is $\psi \approx 40°$, it would seem that mode mixity theory would suggest that $\Gamma_{delam} > \Gamma_{channel}$. This assumes that fracture occurs between ligands of neighboring nanocrystals in both cases (and this seems to be true, since Fig. 7 suggests delamination does not occur directly from the Au film) and that plasticity effects would be the same (which may not be since the layer of nanocrystals under the delamination crack is very thin), so it is not clear if the delamination toughness should be larger here. The experimental error is large enough to preclude drawing any conclusion about this.

V. CONCLUSIONS

We have studied the fracture, strain, and stress of EPD films of CdSe nanocrystals as a function of the film thickness, nanocrystal size, and drying method. Fracture results from the film stress that develops with the loss of residual solvent after EPD when the film exceeds a threshold thickness that increases with nanocrystal core diameter. A hierarchical pattern of wider first generation and then narrower higher-generation cracks is observed after drying and this generational crack formation and a preferred direction for film drying are observed in real time; real-time analysis of fracture will be the subject of another study. Delamination is seen for wider cracks. The toughness is estimated to be ~220–250 J/m^2 for channel cracking and delamination in 3.2 nm nanocrystal films. There is much uncertainty in the toughness values obtained here because of uncertainties in the stresses and strains and the constitutive relations of the fully dried films and in the correctness of using parameters for the dried films because fracture threshold conditions may actually be met during drying. As was also seen in Ref. 5, the ligands play a very important part in the mechanical properties of these nanocrystal films. Further understanding of the nanomechanics of the dried and drying films and the roles of ligands in both will be the subject of future study.

Understanding the nanomechanics at interfaces between nanoscale building blocks represents a complex problem, but one that is still of great importance for ensuring mechanical robustness and film homogeneity over large lateral dimensions. While the classical theories of fracture used here clearly have relevance, improved modeling of fracture, in particular, and of mechanical properties, in general, is needed for nanocrystal films. The issues pertaining to nanoscale interfaces and fracture discussed here are broadly generalizable to other assemblies of nanoscale building blocks, including superlattices, monolayers, and nanocomposite films fabricated by spin coating.

ACKNOWLEDGMENTS

This work was supported primarily by the MRSEC program of the National Science Foundation under Award No. DMR-0213574 and by the New York State Office of Science, Technology, and Academic Research (NYSTAR). Partial support of this project from the NSEC program of the NSF under Award No. CHE-0641523, NSF under Grant No. CMMI-0500239, and NSF under Grant No. DMR-0650555 is also acknowledged. The authors thank Dick Harniman and Ben Smith for experimental assistance.

[1] S. Nizamoglu and H. V. Demir, Nanotechnology **18**, 405702 (2007).
[2] D. C. Oertel, M. G. Bawendi, A. C. Arango, and V. Bulovic, Appl. Phys. Lett. **87**, 213505 (2005).
[3] M. A. Islam and I. P. Herman, Appl. Phys. Lett. **80**, 3823 (2002).
[4] S. Banerjee, S. Jia, D. I. Kim, R. D. Robinson, J. W. Kysar, J. Bevk, and I. P. Herman, Nano Lett. **6**, 175 (2006).
[5] D. Lee, S. Jia, S. Banerjee, J. Bevk, I. P. Herman, and J. W. Kysar, Phys. Rev. Lett. **98**, 026103 (2007).
[6] C. B. Murray, D. J. Norris, and M. G. Bawendi, J. Am. Chem. Soc. **115**, 8706 (1993).
[7] W. W. Yu, L. Qu, W. Guo, and X. Peng, Chem. Mater. **15**, 2854 (2003).
[8] S. Jia, S. Banerjee, and I. P. Herman, J. Phys. Chem. C **112**, 162 (2008).
[9] M. A. Islam, Y. Xia, D. A. J. Telesca, M. L. Steigerwald, and I. P. Herman, Chem. Mater. **16**, 49 (2004).
[10] See EPAPS Document No. E-JAPIAU-105-154908 for information on the drying methods and Dundurs parameters. For more information on EPAPS, see http://www.aip.org/pubservs/epaps.html.
[11] C. L. Yaws, *Handbook of Vapor Pressure* (Gulf Pub. Co., Houston, 1994).
[12] G. D. Scott, Nature (London) **188**, 908 (1960).
[13] G. Y. Onoda and E. G. Liniger, Phys. Rev. Lett. **64**, 2727 (1990).
[14] Z. Neda, K. T. Leung, L. Jozsa, and M. Ravasz, Phys. Rev. Lett. **88**, 095502 (2002).
[15] J. W. Hutchinson and Z. Suo, Adv. Appl. Mech. **29**, 63 (1992).
[16] L. B. Freund and S. Suresh, *Thin Film Materials: Stress, Defect Formation, and Surface Evolution* (Cambridge University Press, Cambridge, England, 2003).
[17] R. M. Bowen, *Introduction to Continuum Mechanics for Engineers* (Plenum, New York, 1989).
[18] W. M. Lai, D. Rubin, and E. Krempl, *Introduction to Continuum Mechanics*, 3rd ed. (Pergamon, New York, 1996).
[19] M. A. Biot, J. Appl. Phys. **12**, 155 (1941).
[20] J. R. Rice and M. P. Cleary, Rev. Geophys. Space Phys. **14**, 227 (1976).
[21] V. B. Shenoy, A. F. Schwartzman, and L. B. Freund, Int. J. Fract. **103**, 1 (2000).

[22]J. L. Beuth, Jr., Int. J. Solids Struct. **29**, 1657 (1992).
[23]M. Y. He, A. G. Evans, and J. W. Hutchinson, Acta Mater. **45**, 3481 (1997).
[24]E. M. Arruda and M. C. Boyce, J. Mech. Phys. Solids **41**, 389 (1993).
[25]M. C. Boyce and E. M. Arruda, Rubber Chem. Technol. **73**, 504 (2000).
[26]P. Hiemenz and R. Rajagopalan, *Principles of Colloid and Surface Chemistry* (Marcel Dekker, Inc., New York, Basel, 1997).
[27]D. W. Smith, *Inorganic Substances: A Prelude to the Study of Descriptive Inorganic Chemistry* (Cambridge University Press, Cambridge, England, 1990).